Biochimica et Biophysica Acta 1838 (2014) 921–931

Contents lists available at ScienceDirect

Biochimica et Biophysica Acta

journal homepage: www.elsevier.com/locate/bbamem

$K_V10.1$ K^+-channel plasma membrane discrete domain partitioning and its functional correlation in neurons☆

Aura M. Jiménez-Garduño [a,b], Miso Mitkovski [c], Ioannis K. Alexopoulos [c], Araceli Sánchez [b], Walter Stühmer [b], Luis A. Pardo [b,*], Alicia Ortega [a,**]

[a] Biochemistry Department, Medicine Faculty, National Autonomous University of Mexico (UNAM), Av. Universidad #3000, 04510 Coyoacán, Mexico City, Mexico
[b] Molecular Biology and Neuronal Signaling Department (MBNS), Max Planck Institute for Experimental Medicine (MPI-EM), Hermann-Rein-Str. 3, 37075 Göttingen, Germany
[c] Light Microscopy Facility, Max Planck Institute for Experimental Medicine (MPI-EM), Hermann-Rein-Str. 3, 37075 Göttingen, Germany

ARTICLE INFO

Article history:
Received 15 April 2013
Received in revised form 27 October 2013
Accepted 5 November 2013
Available online 22 November 2013

Keywords:
$K_V10.1$
Eag1
Cholesterol
Membrane
Cyclodextrin

ABSTRACT

$K_V10.1$ potassium channels are implicated in a variety of cellular processes including cell proliferation and tumour progression. Their expression in over 70% of human tumours makes them an attractive diagnostic and therapeutic target. Although their physiological role in the central nervous system is not yet fully understood, advances in their precise cell localization will contribute to the understanding of their interactions and function. We have determined the plasma membrane (PM) distribution of the $K_V10.1$ protein in an enriched mouse brain PM fraction and its association with cholesterol- and sphingolipid-rich domains. We show that the $K_V10.1$ channel has two different populations in a 3:2 ratio, one associated to and another excluded from Detergent Resistant Membranes (DRMs). This distribution of $K_V10.1$ in isolated PM is cholesterol- and cytoskeleton-dependent since alteration of those factors changes the relationship to 1:4. In transfected HEK-293 cells with a mutant unable to bind Ca^{2+}/CaM to $K_V10.1$ protein, Kv10.1 distribution in DRM/non-DRM is 1:4. Mean current density was doubled in the cholesterol-depleted cells, without any noticeable effects on other parameters. These results demonstrate that recruitment of the $K_V10.1$ channel to the DRM fractions involves its functional regulation.

1. Introduction

The human *ether à-go-go1* protein (Eag1, $K_V10.1$, encoded by *KCNH1*) is a voltage-gated potassium channel and is a member of the EAG family. It is expressed almost exclusively in brain tissue and is involved in cell excitability [1,2], memory processes [1,3] and cell proliferation [4]. The function of $K_V10.1$ in the central nervous system (CNS) is not yet clear, but its biophysical properties have been studied in heterologous systems. These properties, including delayed rectification and low activation voltage [5], as well as its extreme long cytoplasmic regions compared to other non-EAG K_V channels [6], and its expression in highly proliferative tumour tissues suggest that $K_V10.1$ might be involved in non-canonical K^+ channel activities. Several intracellular protein interactions, including its regulation by calmodulin [7], calcium-calmodulin kinase II (CaMKII) [8], rabaptin [9] and cortactin [10], as well as its effect on the hypoxia inducible factor (HIF) expression in heterologous systems [11], imply an involvement with intracellular signalling processes and with cell cycle-related events [12]. Recently, the use of imaging techniques indicated that synaptic $K_V10.1$ localises to the presynaptic membrane [13]; nevertheless, a more detailed description of its PM localisation at this and other locations is still lacking.

The discovery of different lipid phases-like, known as lipid rafts [14], within the PM of eukaryotic cells has changed the understanding of membrane protein dynamics and their interaction with intra- and extracellular proteins [15–19]. Discrete membrane domain formation is promoted not only by the lipid composition but also by the specific localised protein content. The transmembrane protein domains, the cytoplasmic regions interacting with the cytoskeleton and the co-expression and interactions with different proteins have also been shown to participate in the formation of discrete PM domains [20–22]. A higher content of sphingolipids and cholesterol confers to those

Abbreviations: PM, plasma membrane; DRM, detergent resistant membrane; Ca-CaM, calcium calmodulin; CaMKII, calcium calmodulin kinase II; HIF, hypoxia inducible factor; SNARE, Soluble NSF Attachment Protein; HERG, human EAG related gene, HEK, human embryonic kidney; GalCer, galactosylceramide; GM1, monosialotetrahexosylganglioside1; TCA, trichloroacetic acid; Cav-1, caveolin-1; Flot-2, flotilin-2; TfR, transferrin receptor; GM130, Golgi marker 130; TRAPα, translocon associated protein alpha; MBP, myelin basic protein; PLP, proteolipid protein; Lat-A, latrunculin A; BTX, bungarotoxin; RSA, relative specific activity; Gfap, glial fibrillary acidic protein; Alf1, allograft inflammatory factor1; Olig2, oligodendrocyte transcription factor2, Mtap1, microtubule associated protein1; Syn, synaptophysin; LPR-1, lipoprotein receptor-1

* Correspondence to: L.A. Pardo, MBNS, Max-Planck-Institut fürExperimentelle Medizin, Hermann-Rein-Str. 3, 37075 Göttingen, Germany. Tel.: +49 551 3899643; fax: +49 551 3899646.
** Correspondence to: A. Ortega, Departamento de Bioquímica, Facultad de Medicina, Universidad Nacional Autónoma de México, Cd. Universitaria, Av. Universidad #3000, CP 04510, Coyoacán, México- City, Mexico. Tel.: +52 55 56232511; fax: +52 55 56162419.
E-mail addresses: pardo@em.mpg.de (L.A. Pardo), aortega@unam.mx (A. Ortega).

0005-2736/$ – see front matter © 2013 Elsevier B.V. All rights reserved.
http://dx.doi.org/10.1016/j.bbamem.2013.11.007

regions a more hydrophobic, less dynamic environment [23,24] and resistance to non-ionic detergent extraction. This property is the basis of the concept of DRM [25,26]. Functional studies have confirmed that the lipid compartmentalisation in the PM affects the organisation and function of proteins involved in several forms of signalling processes. Examples include the immunological synapse, where the tyrosine kinase Lck found in lipid rafts is activated by the phosphatase CD45 localised in non-rafts [17]; the lateral force transmission of skeletal muscle where the interaction of the membrane protein β-dystroglycan with and the costameric protein dystrophin is dependent on membrane cholesterol content in lipid rafts [16]; the neurological synapse, where most proteins of the Soluble NSF Attachment Protein (SNARE) complex have been shown to be in cholesterol rich domains [27]; and signalling cascades, in which the human EAG-related gene channel (HERG, member of the EAG family) localises to caveolae and participates in a transmembrane signalling complex [15]. In addition to HERG, other voltage-gated ion channels, including $K_v2.1$, $K_V1.5$ and BK_{Ca}, are located in PM subdomains, where their restricted PM localisation influences not only conductance-related functions but also signalling processes [15,28–30]. Because $K_V10.1$ is not detected in any other normal tissue but has been described as a marker in many tumour tissues [31], the question arises as to whether $K_V10.1$ has different functions within the same cell, depending on its partitioning in the lipid subdomains of the plasma membrane.

The aim of this study was to examine the subdomain distribution of the $K_V10.1$-channel in the neural PM isolated from brain tissue as well as in transfected human embryonic kidney cells. We examined the effects of partial membrane cholesterol depletion, membrane cytoskeleton detachment and Ca^{2+}/CaM binding inhibition on the partitioning of $K_V10.1$ within the different domains. We also investigated the effect of MβCD treatment on the K^+ currents. We show two different $K_V10.1$ populations in the membrane, one of which is dependent on membrane cholesterol concentration, actin submembranal cytoskeleton integrity and Ca^{2+}/CaM binding.

2. Materials and methods

2.1. Experimental models

2.1.1. Mice

All animal experiments were performed in compliance with approved animal policies of the Max Planck Institute of Experimental Medicine and the State of Lower Saxony. Adult male wild-type C57BL/6J mice were used for the isolation of brains.

2.1.2. Cells

The HEK-293 cell line was obtained from DSMZ (DSMZ ACC 305, Germany) and maintained according to the instructions of the supplier. Stable transfectants with pTracer-$K_V10.1$ [32] and pTracer-$K_V10.1$-BBS [33] were grown in DMEM/nutrient mixture F-12 with Glutamax-I (Invitrogen) supplemented with 10% foetal calf serum and selected with Zeocin (Calya, 0.3 mg/ml in culture medium). Glial cell primary cultures were obtained from 8 to 10 isolated P0 mice cortices that were dissected (both hemispheres) and maintained in HEPES–DMEM. The cells were dissociated by Trypsin–EDTA digestion at 37 °C for 15 min. The isolated cells were washed three times with DMEM and homogenised through an 18-gauge syringe. The dissociated cells were collected by centrifugation for 5 min at 500 ×*g* and resuspended in fresh DMEM. The cells were maintained in 10 ml flasks for 2 weeks under standard incubator parameters and then harvested and/or subcultured when they reached 80–90% confluence. The HEK-293 cells transiently transfected with the C7-hEag1 mutant (F714S/F717S) were maintained under the same conditions. The C7 mutant is unable to bind one Ca^{2+}/CaM molecule in the C-terminal of $K_V10.1$ and shows a resistance to intracellular calcium inhibition [7].

2.2. RT-PCR of glial cells

The RNA from the cultured cells was isolated using RNeasy (Qiagen, Hilden, Germany) and was reverse transcribed using Super Script (Invitrogen). Real-time PCR was performed using the TaqMan system in a Light Cycler Detector as previously described for $K_V10.1$ detection [31]. For the glial and neuronal markers, primers were selected using the Universal Probe Library (Roche) and detected with SYBR Green.

2.3. Plasma membrane isolation

The plasma membranes from the brain tissue were isolated using a modification of the protocol described by Schindler and Nothwang [34]. Briefly, isolated fresh or frozen (−80 °C) brains were homogenised with a Teflon pestle homogeniser attached to a drill in Buffer A (15 mM Tris–HCl, 320 mM sucrose and EDTA-free protease inhibitor, pH7.8) and centrifuged three times to eliminate nuclei and debris (3000 ×*g*, 10 min, 4 °C). The supernatant was layered over 850 mM sucrose in Buffer A and centrifuged for 30 min at 70,000 ×*g*, at 4 °C. The interface between 320 mM and 850 mM sucrose, which corresponds to myelin cloud [35], was discarded, and the remaining sample was centrifuged for 30 min at 20,000 ×*g*, at 4 °C to eliminate the mitochondria and possible residual myelin. The supernatant was then centrifuged for 1 h at 100,000 ×*g* at 4 °C to sediment the microsomes. The microsomes were resuspended in Buffer A with 250 mM sucrose and used for the wheat germ agglutinin (WGA) binding method of the two-phase affinity system as previously described [34]. To evaluate the final product, enzyme activity assays [36] and Western blotting were performed. The plasma membranes from the cultured cells were isolated using the protocol described by Yao et al. [37].

2.4. Cholesterol depletion and cytoskeleton detachment

Methyl-β-cyclodextrin (MβCD, Sigma-Aldrich) was used to extract the cholesterol from isolated crude membranes or living cells. The purified PM from the brain tissue was incubated with 30 mM MβCD for 1 h at 37 °C with agitation and then washed twice with PBS (pH 7.4). The pellet of the last wash step underwent the DRM isolation protocol. In the case of the HEK-$K_V10.1$ cells, the cells were washed with PBS, trypsinised and divided into 1 ml aliquots of 5–7 million cells each and then incubated with 10 mM MβCD in serum-free medium for 30 min at 37 °C with agitation. The control samples were treated in the same manner substituting PBS for the MβCD. The pellets were subsequently frozen at −80 °C or used directly for the PM and DRM isolation procedures.

2.4.1. Actin cytoskeleton detachment

Sodium carbonate (Na_2CO_3) was used to detach actin from the isolated brain PM. A 500 μl aliquot of PM was incubated with 20 ml of 150 mM Na_2CO_3 for 5 min on ice and then washed once with PBS. The pellet was resuspended in PBS. A 100 μl aliquot was reserved and the remainder of the sample was incubated with 1% Triton X-100 for isolation of the DRM. For the HEK-$K_V10.1$ cells, a similar procedure in which 1 μl of 10 μM Latrunculin A (Lat A, Sigma) dissolved in DMSO replaced the MβCD. The cells were incubated for 1 h at 37 °C with agitation. The control samples were incubated with 1 μl DMSO alone.

2.5. Isolation of detergent-resistant membrane (DRM)

Unless otherwise specified, the tissue or cell PM was resuspended in PBS (pH 7.4), incubated in 1% Triton X-100 for 30 min at 4 °C and then diluted in an equal volume of an 80% sucrose solution. A discontinuous gradient formed by the addition of 30% and 5% sucrose solutions was then centrifuged for 18 h at 200,000 ×*g*, at 4 °C. Nine fractions were recollected from the top to the bottom. The protein content was determined using the bicinchoninic acid (BCA) protein

assay (Pierce), and the fractions were analysed for the presence of monosialotetrahexosylganglioside (GM1) using a dot-blot. For the Western blot analysis, the fractions were pooled into three samples: DRM (fractions 2–4), and non-DRM (fractions 5–6 and 7–9). The same amount of protein of each pooled sample was precipitated using trichloroacetic acid (TCA) [38]. The precipitated proteins were then resuspended in a loading buffer.

2.6. Cholesterol determination

For cholesterol concentration measurement the Cholesterol/Cholesteryl Ester Quantitation Kit (Biovision) was used according to the manufacturer's instructions. Absorbance measurements were performed at 570 nm in a 96-well plate. Cholesterol concentration is expressed in mg cholesterol/mg protein.

2.7. Immunoblotting and densitometry

Protein extracts were separated by gradient SDS-PAGE (either 3–8% Tris–acetate gel or 4–12% Bis–Tris gel, NuPAGE, Invitrogen) and transferred to nitrocellulose membranes (Amersham). For dot-blot assays, 3 μl with the same amount of protein concentration of each fraction was put onto a nitrocellulose membrane and let dry for 15 min. Membranes from either Western blot or dot-blot were blocked at least 30 min with 0.1% casein (Roche Applied Science), 5% non-fat dry milk (Bio-Rad) or 5% BSA (Sigma) and incubated with the corresponding antibody or toxin. Peroxidase conjugated cholera toxin (1:50,000, Sigma), O1 pentameric antibody against galactosylceramide (GalCer) (1:50; a gift from Prof. K.A. Nave, Max-Planck-Institute of Experimental Medicine, Göttingen), Caveolin-1 (Cav-1; 1:300, Polyclonal, Santa Cruz), Flotillin-2 (Flot-2; 1:1000, monoclonal, BD Bioscience), K_V10.1 (1:1500, Polyclonal, 9391; [39]), Transferrin Receptor (TfR; 1:1000, monoclonal, BD Bioscience), Golgi marker (GM130; 1:500, BD), Translocon associated protein alpha subunit (TRAPα; 1:1000, Abcam), Myelin Basic Protein (MBP; 1:1000, Abcam), Proteolipid Protein (PLP, 3F4; 1:250, a gift from Prof. K.A. Nave, Max-Planck-Institute of Experimental Medicine, Göttingen) and Actin (Abcam; 1:1000). After washing and incubation with the corresponding peroxidase-labelled secondary antibody (Invitrogen) if needed, blots were developed using Millipore Immobilon system. Signals for Western blot and dot-blot were detected in a Bio-Rad Chemi-Doc luminescence detection system. Densitometry analysis was performed with ImageJ.

2.8. Electrophysiology

Cells were grown for 24–72 h on poly-L-lysine-coated glass coverslips. For MβCD experiments, cells were incubated in serum-free medium with 30 mM MβCD at room temperature just before the measurements. Macroscopic currents were recorded in the whole-cell configuration of the patch-clamp technique [40] using an EPC-9 amplifier (HEKA). Patch pipettes with a tip resistance of 2–5 MΩ were made from Corning #0010 capillary glass (WPI). Series resistance was compensated by 70%. Internal solution contained (in mM); 100 KCl, 45 N-Methyl-D-Glutamine, 10 1,1-bis(*O*-aminophenoxy)ethane-N, N,N′,N′-tetraacetic acid (BAPTA) tetrapotassium salt, 10 HEPES/HCl, pH 7.35 and the external solution contained (in mM); 160 NaCl, 2.5 KCl, 2 $CaCl_2$, 1 $MgCl_2$, 8 glucose, 10 HEPES/NaOH, pH 7.4. The holding potential for all experiments was −70 mV. Electrophysiological experiments were carried out at room temperature. Data processing and curve fitting were performed with Igor Pro (WaveMetrics). Where applicable, data are presented as the mean ± standard error.

2.9. Affinity cytochemistry and confocal microscopy

For imaging experiments, HEK-293 stably transfected with pTracer-K_V10.1-BBS was used. Cells were grown on 12 mm fibronectin coated coverslips for 48 h and then treated with different drugs. For cholesterol depletion cells were incubated with 5 mM MβCD for 30 min at 37 °C or with PBS. For actin detachment, incubation with 1 μM of Lat A or 1 μl/ml DMSO was performed. After each treatment cells were washed three times with TBS (pH 7.4), incubated with Cholera Toxin-FITC (CT-FITC, Sigma, 1 μl/ml) for 5 min at RT, then briefly suspended in TBS and incubated with Bungarotoxin-Alexa Fluor® 555 (BTX-AF555, Invitrogen, 3 μl/ml) for 15 min at RT, washed three times, fixed with 10% formalin for 10 min at 4 °C, washed 5 times and mounted on slides with ProLong-DAPI (Molecular Probes). Slides were kept overnight at 4 °C and were observed in a Leica SP5 confocal microscope. The image analysis was performed as follows: A Leica SP5 confocal laser-scanning microscope (CLSM, Leica, Mannheim) equipped with hybrid detectors was used to record representative fields of view occupied by cells containing the FITC and BTX-AF555 signals. Care was taken to ensure identical acquisition settings. A macro was generated for the ImageJ software package "Fiji" [41] and applied to quantify fluorescent signal originating from the differently treated cells. Herein, a region of interest (ROI) was drawn manually for each cell, which delineated the lower, planar cell membrane, but excluded cell edges, where the membrane curls upward and is more difficult to quantify due to out-of-focus signal. A binary image of the respective FITC and BTX-AF555 channels was generated by applying the "MidGrey" local thresholding method with a 15-pixel radius [41]. The binary images were then added to generate an image in which the area covered by the overlapping signals could be measured and normalised to the overall ROI area in order to obtain the percent overlapping area. The means were then calculated from 91 CTRL and 92 MβCD-treated cells.

2.10. Statistical analysis

For the statistical analysis we used Excel and StatPlus. For all densitometric and microscopy image analyses ImageJ programme was used and a non-paired two-tailed *t* test was performed. In the case of current recording, analysis was performed with the Igor programme and a non-paired one-tailed *t* test was used.

3. Results

3.1. Purified plasma membranes

Plasma membranes from brain tissue were isolated using a modification of a previously described differential centrifugation and a discontinuous sucrose gradient procedure [34]. The major modification was the addition of a sequential centrifugation step for myelin extraction based on classical isolation methods [42]. Fig. 1 shows the characterisation of the isolated PM. Fig. 1A shows a dot blot for GalCer in the isolated PM compared with the initial homogenate, where only 50% of GalCer was removed. However, after myelin extraction, 94% of the GalCer was removed. Fig. 1B shows that the content of the two major myelin proteins, MBP and PLP, diminished by 35% and 37%, respectively, in the isolated PM relative to the initial homogenate. To further analyse the purity of the final PM fraction, assays of the three major membrane enzymes selective for intracellular membrane sources were performed. Fig. 1C shows that the Relative Specific Activity (RSA) of alkaline phosphatase increased 5-fold in the PM fraction compared with the initial homogenate. The RSA of succinate dehydrogenase was 0.19 ± 0.36 and for NADPH cytochrome c reductase was 0.47 ± 0.08; the RSA was less than one in both cases. Fig. 1D shows Western blots for GM130, a marker for the Golgi membranes, and TRAPα, a marker for the endoplasmic reticulum, in the different membrane fractions. GM130 was absent from the PM fraction, and the TRAPα content in this fraction was reduced to 5% of the signal observed in the initial homogenate. Further analysis of the K_V10.1 membrane distribution was performed in an enriched PM fraction with minimal or no contribution from myelin and inner membranes.

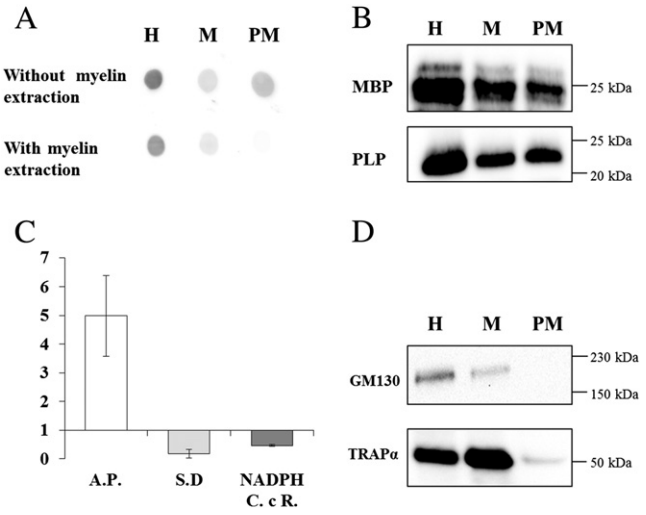

Fig. 1. Characterization of PM fractions isolated from the brain. A) Dot-blot against GalCer in fractions obtained with the original protocol (without myelin extraction) and our modified protocol (with myelin extraction); H: total homogenate, M: microsomes, PM: Plasma membrane fraction. B) Western blot detection of two of the main myelin protein markers MBP (Myelin Binding Protein) and PLP (Proteolipid Protein). C) Enzyme activity assays, expressed as the PM relative activity compared to the total homogenate; AP: Alkaline Phosphatase (PM marker; n = 10, mean ± SD = 4.47 ± 4.47), SD: Succinate Dehydrogenase (mitochondria marker; n=6, 0.48 ± 0.37), NADPH CcR: NADPH Cytochrome c Reductase (endoplasmic reticulum marker; n = 5; 0.43 ± 0.08). D) Western blot detection of the Golgi protein GM130 and the reticulum protein TRAPα in the different membrane fractions.

3.2. K_V10.1 is expressed in neurons but not in glia cells

Neuronal K_V10.1 expression has been widely described [43,44]; however, K_V10.1 expression in glia has not previously been studied. Fig. 2 shows the normalised value of the RT-PCR analysis performed for mouse glia and neuron markers in three different cell cultures. The marker for astrocytes was Glial fibrillary acidic protein (*Gfap*); for microglia, Allograft inflammatory factor-1 (*Alf1*); for oligodendrocytes, Oligodendrocyte transcription factor-2 (*Olig2*); and for neurons, Microtubule-associated protein (*Mtap1*) and synaptophysin (*Syn*). The results showed in three independent cultures of different passages and different distributions of glia cell types, only traces of neuronal RNA could be detected, and the K_V10.1 message was virtually absent (0.012 ± 0.03). These results allow us to interpret the subsequent results as essentially specific to neurons.

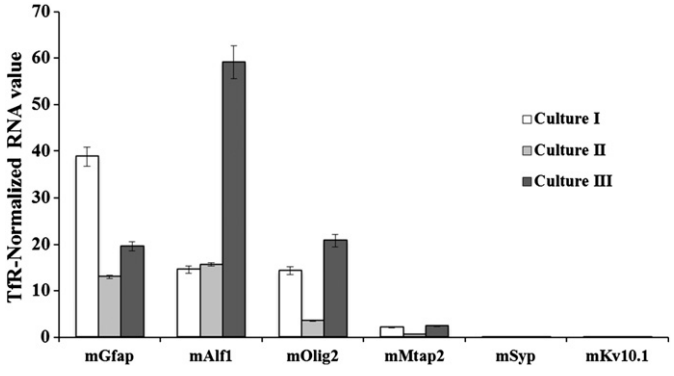

Fig. 2. Characterization of primary mouse glia cell cultures, K_V10.1 is not expressed by glia cells. RT-PCR in three separate cultures enriched in different glia cells. Normalized RNA content with TfR for three different glia markers (mGfap, mAlf1 and mOlig2), two neuron markers (mMtap2 and mSyp) and mK_V10.1.

3.3. Lipid and protein distribution in isolated neuronal plasma membrane from brain tissue

From the purified PM, the DRMs were isolated and characterised. Fig. 3A shows a dot-blot for the ganglioside GM1, which was primarily present in fractions F3 and F4 and absent in fractions F8 and F9. Regarding the specific protein content of the DRM and non-DRM fractions, Fig. 3B shows that TfR was exclusively detected in the non-DRM fractions, while Cav-1 and Flot-2 preferentially localised in the DRM. In the case of K_V10.1, 61% (n = 8) was found in the DRM and the rest in the non-DRM. Fig. 3C shows the protein and cholesterol concentrations of four representative fractions, two corresponding to the DRM (3 and 4) and two to the non-DRM fraction (8 and 9). The DRM fractions accounted only for 9% of the total PM protein concentration, whereas the cholesterol content was 3 times higher in F3 than in the total PM: F3 contained 1.279 ± 0.43 mg chol/mg prot. In contrast, the non-DRM fractions contained 71% of the total protein and a lower cholesterol concentration (fraction 9, 0.167 ± 0.06 mg chol/mg prot). Therefore, there were at least two different populations of K_V10.1 within the neuronal PM, one that partitioned into the DRM subdomain of the PM, enriched in GM1, cholesterol, Cav-1 and Flot-2, and another population that was not associated with the DRM. Co-immunoprecipitation assays to test for a possible physical interaction between Cav-1 and DRM-K_V10.1 were negative (data not shown).

3.4. Neuronal PM-DRM K_V10.1 localisation is dependent on the cholesterol concentration and the integrity of submembrane cytoskeleton

To investigate the factors that determine the distribution of K_V10.1 in the cholesterol-enriched PM subdomains, we isolated DRM from PM previously incubated with 30 mM MβCD to deplete the cholesterol. Fig. 4A–D shows the PM and DRM characterisation after cholesterol depletion. Fig. 4A shows that the MβCD treatment reduced the total PM cholesterol content by 81%; however, this procedure did not substantially alter the GM1 distribution between DRM and non-DRM fractions (Fig. 4B). In terms of protein distribution, the MβCD treatment reduced the content of Cav-1 and Flot-2 in the DRM fractions and increased their concentrations in the non-DRM fractions (Fig. 4C). The extraction of cholesterol with MβCD reduced the cholesterol concentration in the DRM from 1.279 ± 0.43 to 0.100 ± 0.09 mg cholesterol/mg protein in F3, but the concentration in non-DRM fractions was not changed (Fig. 4D). Because DRM proteins such as Cav-1 and Flot-2 interact with the submembrane cytoskeleton proteins in other systems [16], we investigated the importance of the submembrane cytoskeleton integrity on the DRM lipid and protein composition. Fig. 4E–H shows the effect of a basic pH shock with 150 mM Na_2CO_3 (pH 11) on the DRM lipid and protein composition. After the Na_2CO_3 treatment, the PM-associated actin was reduced by 88% (Fig. 4E); the inset in Fig. 4E shows a Western blot of a representative experiment in which TfR was used as an internal control. After the pH shock, GM1 was evenly distributed among the DRM and non-DRM fractions (Fig. 4F). This treatment also caused loss of the signals for Cav-1 and Flot-2 in the DRM fractions and for TfR in the non-DRM fractions (Fig. 4G). As shown in Fig. 4H, cholesterol concentration in the DRM (0.819 ± 0.369 mg chol/mg prot) and the non-DRM (1.095 ± 0.570 mg chol/mg prot) fractions was similar to the concentration in the PM (0.638 ± 0.230 mg chol/mg prot).

Because MβCD and Na_2CO_3 modified the DRM lipid and protein composition, the K_V10.1 distribution was studied following treatment with these agents. Fig. 5A shows a representative Western blot with an anti-K_V10.1 antibody showing changes in the distribution of K_V10.1 in the DRM and non-DRM fractions. Densitometric quantification of the DRM-K_V10.1/non-DRM-K_V10.1 ratio is shown in Fig. 5B. Under the control conditions, the average ratio was 1.74 ± 0.644 (n = 8). This ratio was significantly reduced by both cholesterol depletion (ratio 0.175 ± 0.130; n = 6) and actin detachment (0.153 ± 0.105; n = 3)

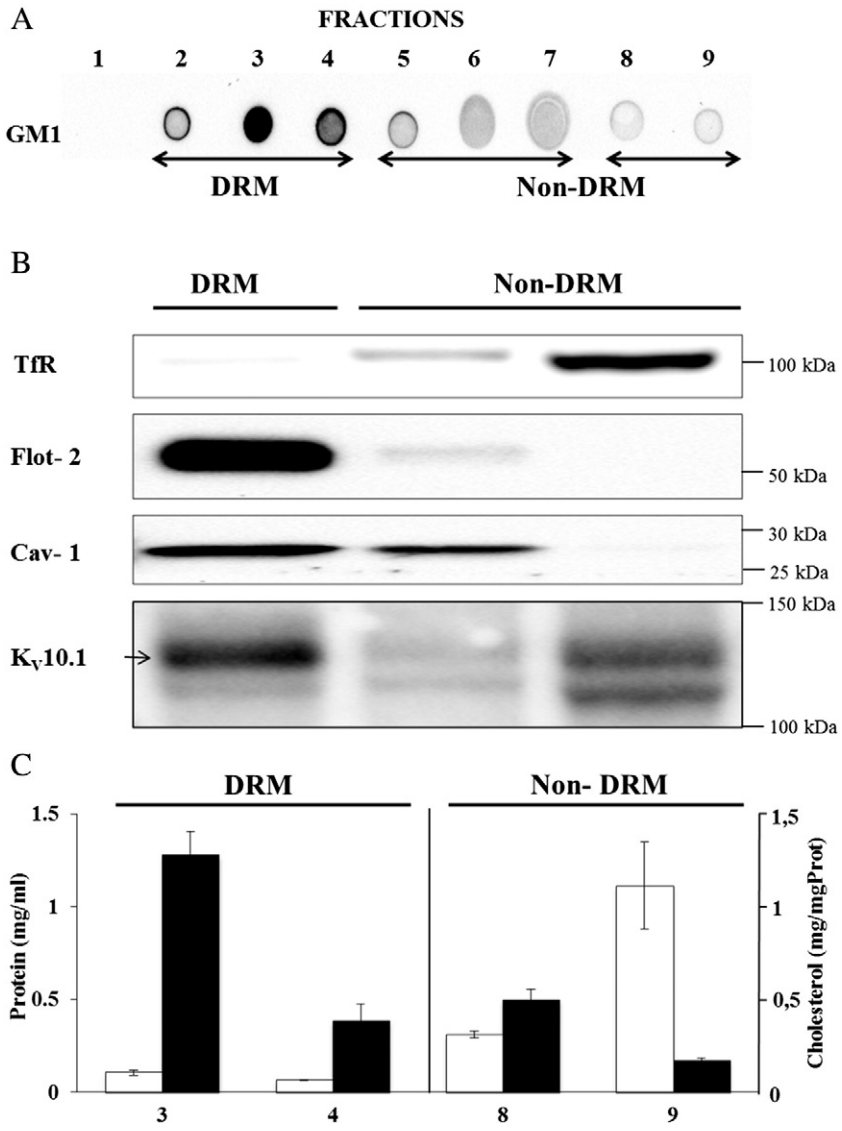

Fig. 3. Characterization of DRM isolated from brain PM, K_V10.1 associates with DRM. A) Dot- blot against GM1 ganglioside in the 9 fractions of the sucrose gradient. DRM are constituted by fractions 2–4. Non-DRM from fractions 5–9 were divided into two: 5–7 and 8,9. B) Distribution of K_V10.1 in the membrane fractions; 60% of K_V10.1 expresses in DRM fractions where two other raft markers are also present (flot-2 and cav-1), the other 40% is found in the lowest non-DRM fraction together with the non-raft marker TfR (n=8). C) Protein concentrations in mg/ml (white columns) of four representative fractions (n=9): *DRM* (Fr:3, 0.11 ± 0.05; Fr:4, 0.06 ± 0.03) and *non-DRM* (Fr:8, 0.31 ± 0.16; Fr:9, 1.11 ± 0.53) and cholesterol concentration in mg Chol/mg Prot (black columns) of the same fractions (n=12): *DRM* (Fr:3, 1.28 ± 0.44; Fr:4, 0.39 ± 0.31) and *non-DRM* (Fr:8, 0.5 ± 0.19; Fr:9, 0.17 ± 0.06).

($p < 0.001$ in both cases). These results strongly indicate that the K_V10.1 relocates from the DRM fraction to the non-DRM fraction after MβCD and Na_2CO_3 treatments. To evaluate the degree of relocation of the DRM-associated K_V10.1 with respect to other DRM- and non-DRM-resident proteins, we calculated the ratios of K_V10.1/Flot-2 and K_V10.1/TfR (Fig. 5C). For the control DRM fractions, the K_V10.1/Flot-2 ratio was 0.697 ± 0.205, and in the non-DRM fractions, the K_V10.1/TfR ratio was 0.433 ± 0.150, in good agreement with the DRM-K_V10.1/non-DRM-K_V10.1 ratio of 3:2. For the MβCD treated membranes we observed a K_V10.1/Flot-2 ratio of 0.155 ± 0.119 in the DRM fractions and a K_V10.1/TfR ratio of 0.9 ± 0.087 for the non-DRM fractions. This result suggests that cholesterol depletion with MβCD has a greater effect on the DRM-associated K_V10.1 than it does on Flot-2. After the removal of the submembranal cytoskeleton with Na_2CO_3, we observed a K_V10.1/Flot-2 ratio of 1.827 ± 0.561 for the DRM fractions and a K_V10.1/TfR ratio of 0.939 ± 0.016 for the non-DRM fractions. Thus, our results show that the submembrane cytoskeleton is needed for proper PM protein partitioning of both K_V10.1 and Flot-2. The effect of the detachment of the submembrane cytoskeletal proteins on K_V10.1 PM partitioning was stronger than the effect of cholesterol depletion. These results indicate that both cholesterol and the submembrane cytoskeleton are key factors determining the K^+ channel distribution in the two populations.

3.5. K_V10.1 localisation in HEK cells is dependent on cholesterol concentration

The effects of MβCD on K_V10.1 membrane distribution in cultured HEK cells can be seen in Fig. 6. Fig. 6A shows a Western blot for K_V10.1 in the DRM and non-DRM fractions after cholesterol depletion with 10 mM MβCD compared to the control. Fig. 6B shows the DRM-K_V10.1/non-DRM K_V10.1 ratios for the control membranes incubated with PBS and the ratio of 0.789 ± 0.382 was compatible with a 2:3 ratio. After cholesterol depletion, the DRM-K_V10.1/non-DRM-K_V10.1 ratio decreased by 58% to 0.330 ± 0.220 ($p < 0.01$). These results, obtained from a cultured cell system, confirm that the cholesterol concentration in the PM is essential for K_V10.1 partitioning into the cholesterol-enriched membrane domains. When the cytoskeleton integrity was altered, we also observed a tendency to decrease the amount of K_V10.1 in the DRM domains, although the difference was

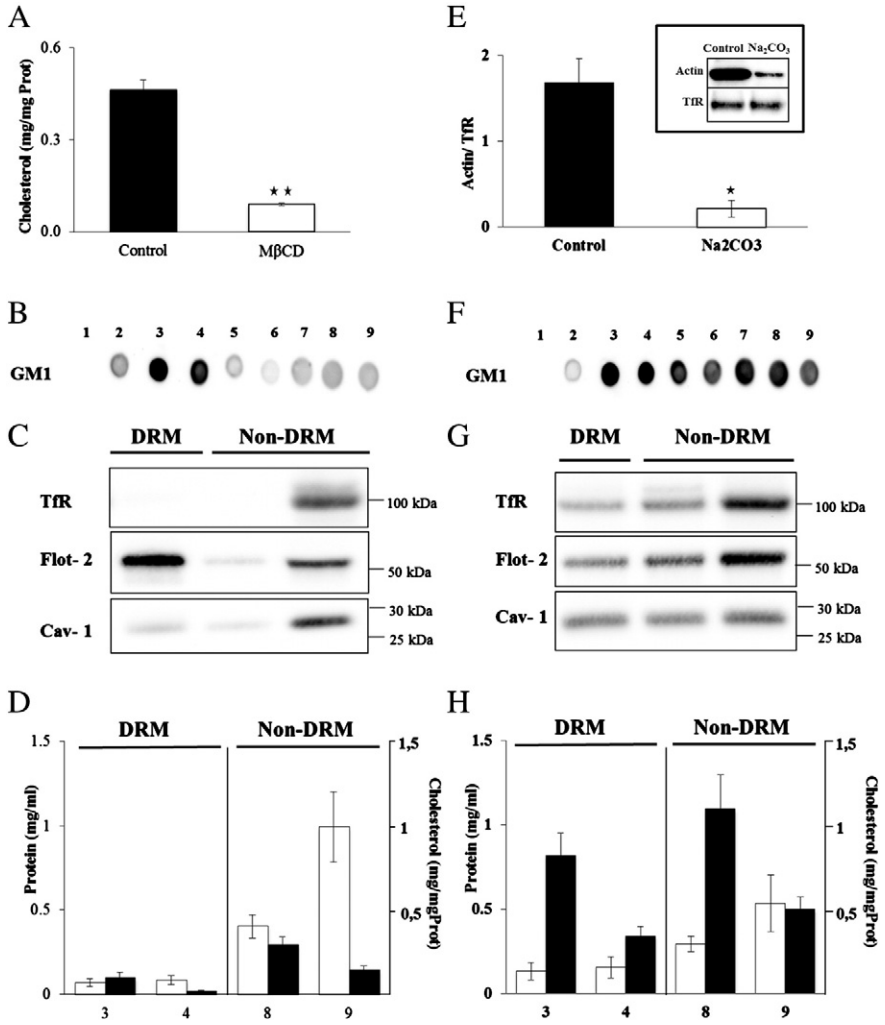

Fig. 4. Brain DRM characterization after cholesterol depletion with MβCD (A–D) and after actin cytoskeleton detachment with Na_2CO_3 (E–H). A) Cholesterol (mg/mg Prot) depletion after 1 h incubation with 30 mM of MβCD. 81% of the inicial amount was extracted from the isolated PM ($n = 8$, control: 0.462 ± 0.1, MβCD: 0.09 ± 0.01, $p < 0.01$). B) Dot-blot against GM1. C) WB showing the distribution of the three domains markers flot-2, cav-1 and TfR in the different fractions. D) Protein concentrations in mg/ml (white columns) of four representative fractions (n=7): *DRM* (Fr:3, 0.07 ± 0.05; Fr:4, 0.09 ± 0.07) and *non-DRM* (Fr:8, 0.4 ± 0.18; Fr:9, 0.99 ± 0.56) and cholesterol concentration in mg chol/mg prot (black columns) of the same fractions (n=8): *DRM* (Fr:3, 0.1 ± 0.08; Fr:4, 0.02 ± 0.02) and *non-DRM* (Fr:8, 0.29 ± 0.13; Fr:9, 0.14 ± 0.07). E) Densitometric analysis of actin detachment (normalized with TfR). Actin decreased in 88%. ($n = 5$, control: 1.69 ± 0.61, natrium carbonate: 0.21 ± 0.21, $p<0.05$). Inset: Representative Western blot of isolated PM after treatment with 150 mM of Na_2CO_3; TfR was used as control. F) Dot-blot against GM1. G) WB showing the distribution of the three domain markers flot-2, cav-1 and TfR in the different fractions. H) Protein concentrations in mg/ml (white columns) of four representative fractions ($n = 3$): *DRM* (Fr:3, 0.13 ± 0.09; Fr:4, 0.15 ± 0.1) and *non-DRM*(Fr:8, 0.29 ± 0.08; Fr:9, 0.53 ± 0.29) and cholesterol concentration in mg Chol/mg Prot (black columns) of the same fractions (n=8): *DRM* (Fr:3, 0.82 ± 0.37; Fr:4, 0.34 ± 0.15) and *non-DRM* (Fr:8, 1.1 ± 0.57; Fr:9, 0.5 ± 0.2).

not statistically significant (data not shown). To further investigate the effect of MβCD on the HEK-K_V10.1 cells, we performed confocal microscopy experiments. Fig. 6C shows representative images of the co-localisation of K_V10.1 (red) and CTX (green) after the MβCD treatment. The statistical analysis is shown in Fig. 6D; a significant decrease in the percent of co-localisation is observed after the MβCD treatment ($p < 0.001$). In the case of Lat A treatment, the overlapping area showed a significant increase (data not showed). In contrast to the brain membranes, the cytoskeleton does not appear to play a key role in the K_V10.1 membrane distribution in the HEK-K_V10.1 cells. We therefore investigated whether other factors could be contributing to the partitioning of these channels in the PM of the HEK-K_V10.1 cells.

3.6. Ca^{2+}/CaM binding modulates Eag1 DRM partitioning in HEK-K_V10.1 cells

We transiently transfected HEK-293 cells with the C7 mutant (see Materials and methods) and isolated the DRM. Fig. 8A and B shows images of a representative Western blot and the plotted ratios, respectively. A reduction in the DRM-associated K_V10.1 is observed, reflected by the decrease of the DRM-K_V10.1/non-DRM-K_V10.1 ratio to 0.233 ± 0.083 ($p < 0.01$). This result strongly suggests that Ca^{2+}/CaM is also a contributing factor for the K_V10.1 partitioning to the raft domains, where presumably the negative current modulation occurs.

3.7. K_V10.1 currents in HEK cells increase after MβCD treatment

To determine the functional correlate of cholesterol depletion, we measured K_V10.1 currents in whole-cell patch clamp experiments before and after MβCD incubation (Fig. 7). After cholesterol extraction, the current density in response to a depolarisation to +60 mV increased by approximately two-fold, from 262.4 ± 25.1 pA/pF ($n = 7$) to 489.8 ± 79.37 pA/pF ($n = 7$, $p < 0.05$); representative recordings are shown in Fig. 7A and B. In the current–voltage relationship shown in Fig. 7C, it can be appreciated that the increase was already significant in the range from +20 mV to +80 mV. Because the activation time constant of K_V10.1 shows a characteristic dependence on pre-pulse potential [45], we also measured the 20–80% rise time of currents elicited by a depolarisation to +40 mV after 5 s prepulses to −120 or −60 mV. Cholesterol extraction did not affect the time required for the channel to

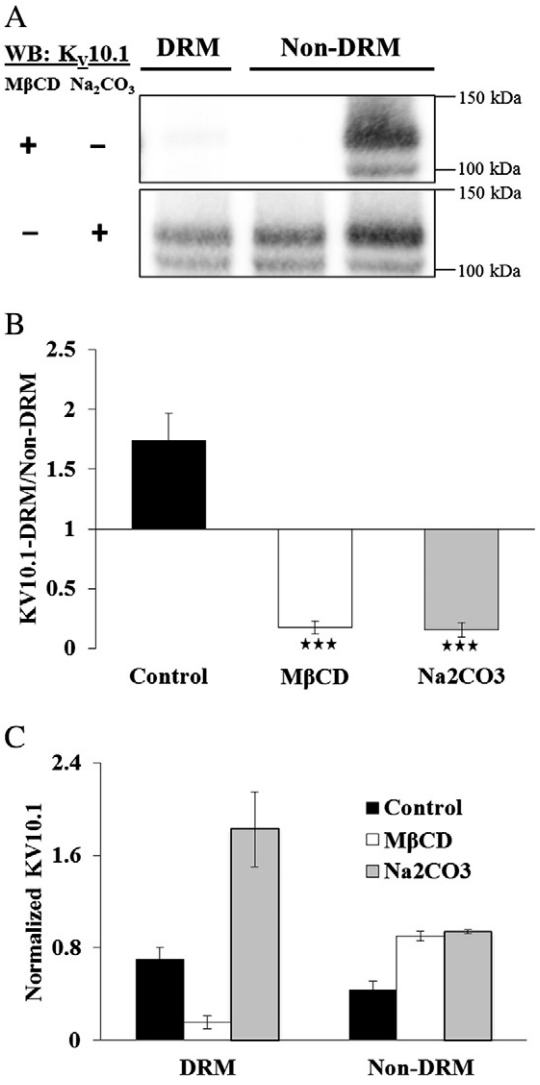

Fig. 5. Brain $K_V10.1$ membrane distribution is affected by cholesterol depletion and actin cytoskelton disturbance. A) Western blot against $K_V10.1$ in the different fractions after treatment with MβCD and Na_2CO_3. B) $K_V10.1$ ratio between the amount of $K_V10.1$ in DRM divided by the amount in $K_V10.1$-non-DRM in control (n = 8, 1.74 ± 0.64) and MβCD (n = 6, 0.18 ± 0.13) and Na_2CO_3 (n = 3, 0.15 ± 0.1) treated membranes. C) $K_V10.1$ percentage normalized with the loading control of each fraction. For DRM the percentage of flotilin was used (*control*: n=4, 0.7 ± 0.2; mβcd: n = 5, 0.15β0.12; *Na_2CO_3*: n=3, 1.83 ± 0.56), for non-DRM TfR percentage was used. (control: n = 4, 0.43 ± 0.15; mβcd: n = 5, 0.9 ± 0.08; sodium carbonate: n = 3, 0.94 ± 0.03).

reach the open state. These results, together with our previous study [46], suggest that cytoskeleton integrity and cholesterol concentration participate as stabilising factors for $K_V10.1$ currents. Specifically, when these factors are disturbed, the currents increase.

4. Discussion

In the present study, we demonstrate that 1) $K_V10.1$ is expressed in neural but not in glial cells of mice; 2) two populations of $K_V10.1$ partition into different membrane domains; 3) partitioning to the DRM depends on cholesterol, the cytoskeleton and Ca^{2+}/CaM; and 4) cholesterol depletion increases $K_V10.1$ K^+ current density in HEK-$K_V10.1$ cells.

4.1. $K_V10.1$ is expressed in neural cells

The expression of $K_V10.1$ in neurons has been demonstrated using in situ hybridisation and immunohistochemistry, but expression in glial cells has not been specifically addressed [13,43,44]. We did not observe expression of $K_V10.1$ in cultured mouse glia cells. This result is specifically interesting because over 50% of human gliomas express $K_V10.1$ [47]. Thus, the presence of $K_V10.1$ appears to be an abnormal acquired expression in gliomas, as it is in other solid tumours [31].

4.2. Partitioning of $K_V10.1$ in plasma membrane subdomains

Several proteins, such as caveolins, flotillins, Src, Lck, Rab11, H-Ras, dystroglycans, BK channels, HERG, Kv1.5, Kv1.4 and Kv4.3 are known to associate with detergent-resistant membrane domains enriched in cholesterol and sphingolipids, while other transmembrane proteins such as TfR, calnexin, Na^+/K^+ ATPase, K-ras, $K_V3.2$ and $K_V4.2$ are excluded from these membrane domains [19,29,48–59]. Our results indicate that the $K_V10.1$ present in PM isolated from neurons distributes between the DRM and non-DRM fractions, suggesting the existence of at least two populations of the protein with respect to their affinity to interact with specific lipids and proteins. Whether $K_V10.1$ partitioning into the DRM is a stable or a transient state needs to be further investigated. $K_V10.1$ thus belongs to the group of K-channels, such as Kir2 [60], $K_V2.1$ [55] and $K_V4.1$ [56], that have also been shown to partition to the DRM as well as to the non-DRM domains. In order to reside in the DRM, the length of a transmembrane segment must match the thickness of the cholesterol-enriched membranes [61–63]. This depends on protein sequence, but changes in protein conformation can also induce mismatching with membrane thickness and therefore result in exclusion. Such conformational changes can be an effect of protein–protein and protein–lipid interactions. For example, the kinase PKC-βII associates with DRM, depending on the co-expression of the protein ZAP70 in leukaemia cells [22]. The Low Density Lipoprotein Receptor 1 (LPR-1) resides in the non-DRM domains in cultured fibroblasts and epithelial cells but is present in the DRM isolated from a smooth muscle cell line [64]. This evidence indicates that the distribution process of membrane proteins involves a more complex regulation than the amino acid sequence alone. The factors involved in this regulation could include post-translational events (phosphorylation and glycosylation), protein–protein interactions within membrane domains, as the case of CD45 and Lck associations within the immunological synapse [17] or interactions between membrane proteins and cytoskeletal proteins as has been shown for the transmission of the lateral force between β-dystroglycan and dystrophin in skeletal muscle [16]. In any case, different membrane distributions of a protein are incompatible with identical structures and conformations.

4.3. $K_V10.1$ PM distribution is dependent on cholesterol, cytoskeleton integrity and Ca^{2+}/CaM binding

Cholesterol extraction with MβCD revealed a close relationship between the concentration of this lipid and DRM/non-DRM partitioning of $K_V10.1$ in brain and HEK cells. Although MβCD has a direct effect on cholesterol and an indirect effect on glycolipids (GM1) and proteins, there are reports that demonstrate that a fraction of the sphingolipid core domain remains buoyant after cholesterol depletion [65]. We observed the same effect in our experiments (Fig. 5B), in which isolation of GM1-rich fractions was still possible despite the extraction of membrane cholesterol. There are several examples that demonstrate that the extraction of cholesterol with MβCD varies widely among membrane proteins and cell systems. Our results show that 30 mM MβCD reduces the cholesterol content in isolated neural PM by 80%, but only 10 mM of MβCD is required to obtain the same effect in cultured HEK-$K_V10.1$ cells. In other tissues, including the skeletal muscle, a 10 mM concentration of the same compound reduces the membrane cholesterol by only 12% but has a large effect on muscle contractility [16]. Furthermore, different proteins may behave differently after MβCD treatment. For example, some proteins such as Lck dissociate completely from the DRM after cholesterol depletion, while others, including the antigen Thy-1 [65] and Flot-2, dissociate only partially

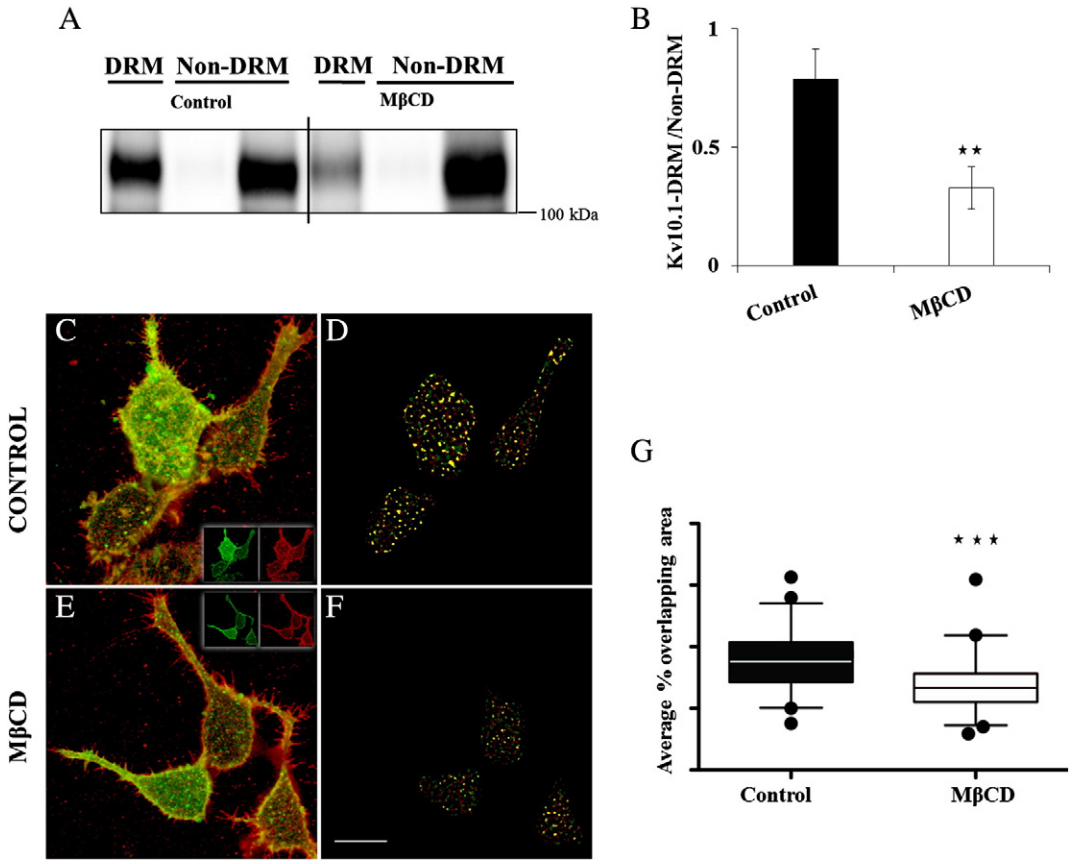

Fig. 6. K_V10.1 membrane distribution is affected by cholesterol depletion in HEK-K_V10.1 cells. A) Western blot against K_V10.1 in the fractions of isolated PM from HEK- K_V10.1 after treatment with PBS or 10mM MβCD. B) K_V10.1 ratio between K_V10.1-DRM and the K_V10.1-non-DRM of control and treated membranes ($n = 6$, $p < 0.01$). C and E) Merged confocal microscopy images of HEK-BBS-K_V10.1 cells marked with bungarotoxin-AlexaFluorâ 555 for K_V10.1 signal (red) and CT-FITC for GM1 signal (green), treated with PBS or 5 mM of MβCD; scalebar: 10 μm; Inset: Single channel images for each staining. D and F) Binary masks indicating the location of either single-stained BTX-AF555 (red) or GM1 (green) pixels, as well as areas in which both stains are present (yellow). G) Comparison of the percent overlapping area between Kv10.1 and GM1 treated with either PBS (control, $n = 91$) or MβCD ($n = 92$) in cells originating from three different experiments ($p < 0.0001$).

even after complete cholesterol extraction. The present study shows that K_V10.1 belongs to the second group. Because no direct interaction of K_V10.1 with cav-1 was found, it seemed unlikely that cholesterol alone determined the location of K_V10.1 at DRM; therefore, we looked for additional regulating factors.

Although it was not evident when the first lipid raft model was proposed [66], it is now accepted that in addition to the lipid content, the proteins associated with the PM are important for stabilising the domain structures. Actin is the key regulator for clustering the proteins in "islands" independent of the lipid content [67]; thus, the PM-bound cytoskeleton and transmembrane protein pickets form fences dividing the cell surface into compartments of 40–300 nm [68]. Experiments with Lat A and Cytochalasin B indicate that the actin meshwork integrity is important for the association of certain proteins including acetylcholine receptors and anion, calcium, and potassium channels with the DRM [69–72]. In our study, the use of Na_2CO_3 removed almost 90% of the attached actin from the brain tissue PM. We show that in the absence of the underlying protein structure, neuronal membranes lose their original organisation (Fig. 5E–H), domains are drastically disrupted and their detergent resistance is altered. These results are in good agreement with the mesoscale membrane model, which states that the cytoskeleton-defined compartments are the highest hierarchical level of the PM in determining and limiting the behaviour of the lipid phases [68]. However, the role of the cytoskeleton integrity in the association of K_V10.1 with the DRM in the HEK cells appears to be different; both biochemical and confocal microscopy results strongly indicate that the association of K_V10.1 with the DRM remains, despite the effects of Lat A on actin polymerisation. Such disparities could be attributed to the differences in the cytoskeleton structure of the two types of cells. In support to this concept, radixin, a protein that connects the α5-GABA A receptor to the actin cytoskeleton in brain tissue, does not interact with the receptor when analysed in HEK-293 transfected cells [73]. It has been reported that the targeting of the alpha 2c adrenoreceptor depended not only on the cell type but also on the differentiation state of a neuroendocrine cell line [74]. The different interactions between K_V10.1 and the cytoskeletal proteins that might be taking place in neurons compared to the HEK-K_V10.1 cells could account for the differences observed in the channel dependence on actin integrity for DRM association.

Finally, we asked whether another factor besides cholesterol could contribute to K_V10.1 PM partitioning in HEK-K_V10.1 cells. Both the N- and the C-terminal domains of K_V10.1 have very well defined binding sites for Ca^{2+}/CaM and a mutant channel (C7) resistant to the Ca^{2+}-CaM binding effect has already been described [7,75]. We analysed the PM partitioning of K_V10.1 when the C7 mutant was transfected to HEK-293 cells, and we observed a reduction in the DRM-associated K_V10.1 (Fig. 8). Although this is the first report where the binding of Ca^{2+}/CaM is explicitly tested as a determining factor for a raft-protein association, a closer examination into the literature provides additional evidence indicating that this can be a general feature of CaM-binding proteins. Du and co-workers reported that association of CaMKII mutants lacking the CaM binding site (291–301) to raft domains was partial or absent [76], compared to the behaviour of wild-type CaMKII [77]. Similarly, only the Ca^{2+}-sensitive adenylyl cyclases partition to membrane rafts, and the cytosolic domains (CaM binding sites) and not the transmembrane spans are responsible for their partitioning

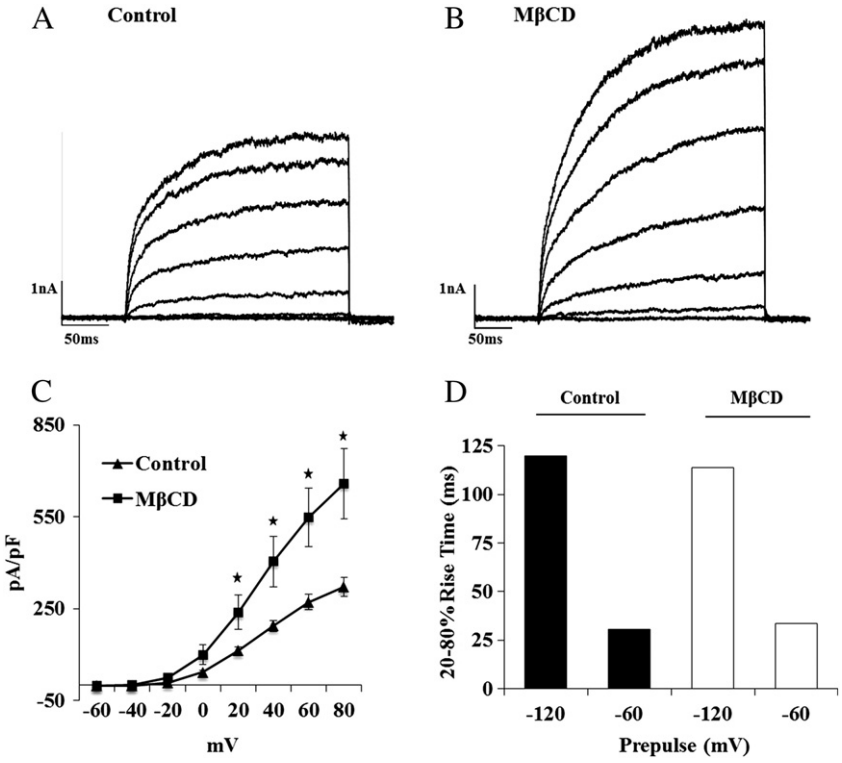

Fig. 7. K_V10.1 density current increases after MβCD treatment. Representative whole cell recordings in HEK- K_V10.1 cells A) control and B) in 30 mM MβCD. C) Graphical representation of the current density at different depolarizing stimuli; from +20 mV to +80 mV the increase is statistically significant ($p < 0.05$, $n = 7$). D) Time to rise of control and treated cells after a 500 ms hyperpolarization pre-pulse and a depolaritzation to +40 mV; no difference in the opening time is observed after cholesterol depletion.

[21]. It is not yet clear why Ca^{2+}-binding proteins would play a role in the regulation of the localisation of some lipid raft proteins. However, calcium is able to bind to the membrane and diminish the flip-flop rate of lipids, a condition that supports the gel state [78]. Furthermore, it has been demonstrated that an increase in the intracellular Ca^{2+} is a contributing, but not necessary, factor for changes in the phospholipid content of leukaemia cells [79]. Together with our results, these findings suggest that Ca^{2+} and/or Ca^{2+}/CaM could play a role in the regulation of some protein or lipid partitioning within the PM. The fact that Ca^{2+} channels and many Ca^{2+}-regulating proteins such as calsequestrin, calreticulin and Ca^{2+} pumps reside inside these domains [21,71,80] could explain the tight regulation of the Ca^{2+} concentrations in those localised regions of the membrane.

4.4. Cholesterol-dependent K^+-current density in HEK-K_V10.1 cells

After cholesterol depletion with MβCD, the current density of HEK-K_V10.1 cells increases significantly (Fig. 8A and B). We also demonstrate that the disruption of cytoskeleton through the inhibition of actin polymerisation is associated with a delocalisation of GM1, K_V10.1, flot-2 and cav-1 from the DRM domains. Disturbance of actin cytoskeleton with cytochalasin B also increases the current density of K_V10.1-transfected CHO cells [46]. One interpretation of these observations is that perturbations of the membrane structure by either cholesterol depletion or cytoskeleton-disrupting agents induce an increase in current due to dissociation of the K_V10.1 protein from the DRM. If this is the case, the DRM-associated K_V10.1, which accounts for approximately 60% of all PM K_V10.1, would not contribute to the total current recorded, and DRM domains would constitute a discrete domain where K_V10.1 might be stored or exert a different DRM-related function. This behaviour is shared by other channels, for example HERG, K_V1.5, BK and Ca_V2.2 [57,71,81,82]. K_V2.1 channels are organised into clusters ("corrals") where they do not contribute to the whole cell current [83]. In general, changes in lipids and anchoring of proteins can influence the electromechanical properties of channels. In the case of the nicotinic acetylcholine receptor [84], changes in the fatty acid and steroid content of the membrane are responsible for the transition between the resting and desensitised states. Direct contact between the lipids and transmembrane regions of this receptor has been described, and the membrane is proposed as a key player for the fine-tuning of the channel activity within specific submembrane domains [85].

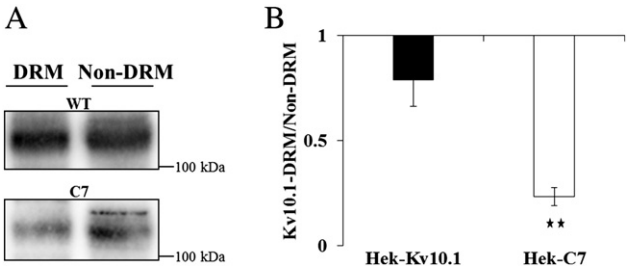

Fig. 8. DRM distribution of the C7 K_V10.1 mutant in HEK-293 cells. A) Western blot against K_V10.1 in HEK- K_V10.1 and HEK-C7 cells after DRM isolation. B) K_V10.1 ratio between the amount of K_V10.1 in DRM and the amount in K_V10.1-non-DRM in control ($n = 9$, 0.79 ± 0.13) and C7 ($n = 4$, 0.23 ± 0.04, $p < 0.01$) cells.

5. Conclusion

In isolated PM from neuronal tissue, K_V10.1 is segregated into two different populations, one associated with the DRM and dependent on the PM cholesterol and on the actin–cytoskeleton and to Ca^{2+}/CaM in PM from transfected HEK-293 cells, with a mutant unable to bind Ca^{2+}/CaM to Kv10.1 protein, and another associated with non-DRM fraction. The partition of K_V10.1 to the different PM DRM/non-DRM seems to play a role in the regulation of its conductive properties as it is dependent on cholesterol in PM of living cells.

Acknowledgements

We wish to thank the Consejo Nacional de Ciencia y Tecnología (CONACyT; #267035) in Mexico and the Deutsche Akademische Austausch Dienst (DAAD; #A/08/74166) in Germany and the Dirección General del Personal Académico, Universidad Nacional Autónoma de México (UNAM-DGAPA-IN219812) for their financial support to AMJG during her PhD programme (Programa de Doctorado en Ciencias Biomédicas, Universidad Nacional Autónoma de México); Dr. Roser Ufartes and Sabine Martin for helpful suggestions on the manuscript; Sabine Klöppner, Barbara Scheufler, Tanja Nilson, Ursula Kutzke, Bärbel Heidrich and Victor Díaz for technical support. We thank Pavel Vazquez (PAVNET) for the design of the graphical abstract.

References

[1] W.D. Kaplan, W.E. Trout III, The behavior of four neurological mutants of *Drosophila*, Genetics 61 (2) (1969) 399–409.
[2] V. Budnik, Y. Zhong, C.F. Wu, Morphological plasticity of motor axons in *Drosophila* mutants with altered excitability, J. Neurosci. 10 (11) (1990) 3754–3768.
[3] J.E. Engel, C.F. Wu, Genetic dissection of functional contributions of specific potassium channel subunits in habituation of an escape circuit in *Drosophila*, J. Neurosci. 18 (6) (1998) 2254–2267.
[4] L.A. Pardo, et al., Oncogenic potential of EAG K(+) channels, EMBO J. 18 (20) (1999) 5540–5547.
[5] A. Bruggemann, et al., Ether-a-go-go encodes a voltage-gated channel permeable to K^+ and Ca^{2+} and modulated by cAMP, Nature 365 (6445) (1993) 445–448.
[6] T. Occhiodoro, et al., Cloning of a human ether-a-go-go potassium channel expressed in myoblasts at the onset of fusion, FEBS Lett. 434 (1–2) (1998) 177–182.
[7] R. Schonherr, K. Lober, S.H. Heinemann, Inhibition of human ether a go-go potassium channels by Ca(2+)/calmodulin, EMBO J. 19 (13) (2000) 3263–3271.
[8] L.C. Griffith, et al., Calcium/calmodulin-dependent protein kinase II and potassium channel subunit EAG similarly affect plasticity in *Drosophila*, Proc. Natl. Acad. Sci. U. S. A. 91 (21) (1994) 10044–10048.
[9] M. Ninkovic, et al., Physical and functional interaction of KV10.1 with Rabaptin-5 impacts ion channel trafficking, FEBS Lett. 586 (19) (2012) 3077–3084.
[10] S. Herrmann, et al., Cortactin controls surface expression of the voltage-gated potassium channel K(V)10.1, J. Biol. Chem. 287 (53) (2012) 44151–44163.
[11] B.R. Downie, et al., Eag1 expression interferes with hypoxia homeostasis and induces angiogenesis in tumors, J. Biol. Chem. 283 (52) (2008) 36234–36240.
[12] L.A. Pardo, et al., Cell cycle-related changes in the conducting properties of r-Eag K^+ channels, J. Cell Biol. 143 (3) (1998) 767–775.
[13] D. Gomez-Varela, et al., Characterization of Eag1 channel lateral mobility in rat hippocampal cultures by single-particle-tracking with quantum dots, PLoS One 5 (1) (2010) e8858.
[14] H.J. Kaiser, et al., Order of lipid phases in model and plasma membranes, Proc. Natl. Acad. Sci. U. S. A. 106 (39) (2009) 16645–16650.
[15] A. Cherubini, et al., Human ether-a-go-go-related gene 1 channels are physically linked to beta1 integrins and modulate adhesion-dependent signaling, Mol. Biol. Cell 16 (6) (2005) 2972–2983.
[16] J. Vega-Moreno, et al., Cholesterol depletion uncouples beta-dystroglycans from discrete sarcolemmal domains, reducing the mechanical activity of skeletal muscle, Cell. Physiol. Biochem. 29 (5–6) (2012) 905–918.
[17] C. Irles, et al., CD45 ectodomain controls interaction with GEMs and Lck activity for optimal TCR signaling, Nat. Immunol. 4 (2) (2003) 189–197.
[18] C. Irles, et al., Plasma membrane subdomain partitioning of Lck in primary human T lymphocytes, Can. J. Physiol. Pharmacol. 88 (4) (2010) 487–496.
[19] H. Zhao, et al., Neurite outgrowth is dependent on the association of c-Src and lipid rafts, Neurochem. Res. 34 (12) (2009) 2197–2205.
[20] S. Lebreton, S. Paladino, C. Zurzolo, Selective roles for cholesterol and actin in compartmentalization of different proteins in the Golgi and plasma membrane of polarized cells, J. Biol. Chem. 283 (43) (2008) 29545–29553.
[21] A.J. Crossthwaite, et al., The cytosolic domains of Ca^{2+}-sensitive adenylyl cyclases dictate their targeting to plasma membrane lipid rafts, J. Biol. Chem. 280 (8) (2005) 6380–6391.
[22] C.M. zum Buschenfelde, et al., Recruitment of PKC-betaII to lipid rafts mediates apoptosis-resistance in chronic lymphocytic leukemia expressing ZAP-70, Leukemia 24 (1) (2010) 141–152.
[23] K. Bacia, et al., Fluorescence correlation spectroscopy relates rafts in model and native membranes, Biophys. J. 87 (2) (2004) 1034–1043.
[24] C. Eggeling, et al., Direct observation of the nanoscale dynamics of membrane lipids in a living cell, Nature 457 (7233) (2009) 1159–1162.
[25] E. London, D.A. Brown, Insolubility of lipids in Triton X-100: physical origin and relationship to sphingolipid/cholesterol membrane domains (rafts), Biochim. Biophys. Acta 1508 (1–2) (2000) 182–195.
[26] J. Sot, et al., Detergent-resistant, ceramide-enriched domains in sphingomyelin/ceramide bilayers, Biophys. J. 90 (3) (2006) 903–914.
[27] T. Lang, SNARE proteins and 'membrane rafts', J. Physiol. 585 (Pt 3) (2007) 693–698.
[28] R.H. Scannevin, et al., Identification of a cytoplasmic domain important in the polarized expression and clustering of the Kv2.1 K^+ channel, J. Cell Biol. 135 (6 Pt 1) (1996) 1619–1632.
[29] J.R. Martens, K. O'Connell, M. Tamkun, Targeting of ion channels to membrane microdomains: localization of KV channels to lipid rafts, Trends Pharmacol. Sci. 25 (1) (2004) 16–21.
[30] A.K. Weaver, et al., BK channels are linked to inositol 1,4,5-triphosphate receptors via lipid rafts: a novel mechanism for coupling [Ca(2+)](i) to ion channel activation, J. Biol. Chem. 282 (43) (2007) 31558–31568.
[31] B. Hemmerlein, et al., Overexpression of Eag1 potassium channels in clinical tumours, Mol. Cancer 5 (2006) 41.
[32] R.E. Garcia-Ferreiro, et al., Mechanism of block of hEag1 K^+ channels by imipramine and astemizole, J. Gen. Physiol. 124 (4) (2004) 301–317.
[33] T. Kohl, et al., Rapid internalization of the oncogenic K^+ channel K(V)10.1, PLoS One 6 (10) (2011) e26329.
[34] J. Schindler, H.G. Nothwang, Enrichment of brain plasma membranes by affinity two-phase partitioning, Methods Mol. Biol. 528 (2009) 119–126.
[35] J.N. Larocca, W. Norton, Isolation of myelin, Current Protocols in Cell Biology, John Wiley & Sons, 2007, pp. 1–19, (3.25).
[36] J. Schindler, et al., Proteomic analysis of brain plasma membranes isolated by affinity two-phase partitioning, Mol. Cell. Proteomics 5 (2) (2006) 390–400.
[37] Y. Yao, et al., The differential protein and lipid compositions of noncaveolar lipid microdomains and caveolae, Cell Res. 19 (4) (2009) 497–506.
[38] E. Kirchner, K. Gruhn, Comparative investigations on the precipitation behavior of various protein precipitates in organs and tissues, Nahrung 29 (7) (1985) 703–709.
[39] Y. Chen, et al., Functional K(v)10.1 channels localize to the inner nuclear membrane, PLoS One 6 (5) (2011) e19257.
[40] O.P. Hamill, et al., Improved patch-clamp techniques for high-resolution current recording from cells and cell-free membrane patches, Pflugers Arch. 391 (2) (1981) 85–100.
[41] J. Schindelin, et al., Fiji: an open-source platform for biological-image analysis, Nat. Methods 9 (7) (2012) 676–682.
[42] H. Jurevics, et al., Normal metabolism but different physical properties of myelin from mice deficient in proteolipid protein, J. Neurosci. Res. 71 (6) (2003) 826–834.
[43] M.J. Saganich, E. Machado, B. Rudy, Differential expression of genes encoding subthreshold-operating voltage-gated K^+ channels in brain, J. Neurosci. 21 (13) (2001) 4609–4624.
[44] S. Martin, et al., Eag1 potassium channel immunohistochemistry in the CNS of adult rat and selected regions of human brain, Neuroscience 155 (3) (2008) 833–844.
[45] J. Ludwig, et al., Functional expression of a rat homologue of the voltage gated either a go-go potassium channel reveals differences in selectivity and activation kinetics between the *Drosophila* channel and its mammalian counterpart, EMBO J. 13 (19) (1994) 4451–4458.
[46] J. Camacho, et al., Cytoskeletal interactions determine the electrophysiological properties of human EAG potassium channels, Pflugers Arch. 441 (2–3) (2000) 167–174.
[47] S. Patt, et al., Expression of ether a go-go potassium channels in human gliomas, Neurosci. Lett. 368 (3) (2004) 249–253.
[48] P. de Diesbach, et al., Differential subcellular membrane recruitment of Src may specify its downstream signalling, Exp. Cell Res. 314 (7) (2008) 1465–1479.
[49] L. Rajendran, S. Le Lay, H. Illges, Raft association and lipid droplet targeting of flotillins are independent of caveolin, Biol. Chem. 388 (3) (2007) 307–314.
[50] P.H. Lommerse, et al., Single-molecule diffusion reveals similar mobility for the Lck, H-ras, and K-ras membrane anchors, Biophys. J. 91 (3) (2006) 1090–1097.
[51] H. Niv, et al., Activated K-Ras and H-Ras display different interactions with saturable nonraft sites at the surface of live cells, J. Cell Biol. 157 (5) (2002) 865–872.
[52] L.J. Foster, C.L. De Hoog, M. Mann, Unbiased quantitative proteomics of lipid rafts reveals high specificity for signaling factors, Proc. Natl. Acad. Sci. U. S. A. 100 (10) (2003) 5813–5818.
[53] M.J. Yu, et al., Large-scale quantitative LC–MS/MS analysis of detergent-resistant membrane proteins from rat renal collecting duct, Am. J. Physiol. Cell Physiol. 295 (3) (2008) C661–C678.
[54] K.M. O'Connell, J.R. Martens, M.M. Tamkun, Localization of ion channels to lipid Raft domains within the cardiovascular system, Trends Cardiovasc. Med. 14 (2) (2004) 37–42.
[55] K.M. O'Connell, M.M. Tamkun, Targeting of voltage-gated potassium channel isoforms to distinct cell surface microdomains, J. Cell Sci. 118 (Pt 10) (2005) 2155–2166.
[56] F. Xia, et al., Targeting of voltage-gated K^+ and Ca^{2+} channels and soluble N-ethylmaleimide-sensitive factor attachment protein receptor proteins to cholesterol-rich lipid rafts in pancreatic alpha-cells: effects on glucagon stimulus-secretion coupling, Endocrinology 148 (5) (2007) 2157–2167.
[57] J. Lin, et al., The regulation of the cardiac potassium channel (HERG) by caveolin-1, Biochem. Cell Biol. 86 (5) (2008) 405–415.
[58] J.R. Martens, et al., Differential targeting of Shaker-like potassium channels to lipid rafts, J. Biol. Chem. 275 (11) (2000) 7443–7446.
[59] R.S. Lam, A.R. Shaw, M. Duszyk, Membrane cholesterol content modulates activation of BK channels in colonic epithelia, Biochim. Biophys. Acta 1667 (2) (2004) 241–248.
[60] S. Tikku, et al., Relationship between Kir2.1/Kir2.3 activity and their distributions between cholesterol-rich and cholesterol-poor membrane domains, Am. J. Physiol. Cell Physiol. 293 (1) (2007) C440–C450.
[61] A. Kundu, et al., Transmembrane domain of influenza virus neuraminidase, a type II protein, possesses an apical sorting signal in polarized MDCK cells, J. Virol. 70 (9) (1996) 6508–6515.
[62] A.G. Lee, Lipid–protein interactions in biological membranes: a structural perspective, Biochim. Biophys. Acta 1612 (1) (2003) 1–40.
[63] T.J. McIntosh, A. Vidal, S.A. Simon, Sorting of lipids and transmembrane peptides between detergent-soluble bilayers and detergent-resistant rafts, Biophys. J. 85 (3) (2003) 1656–1666.

[64] L. Wu, S.L. Gonias, The low-density lipoprotein receptor-related protein-1 associates transiently with lipid rafts, J. Cell. Biochem. 96 (5) (2005) 1021–1033.
[65] S. Ilangumaran, D.C. Hoessli, Effects of cholesterol depletion by cyclodextrin on the sphingolipid microdomains of the plasma membrane, Biochem. J. 335 (Pt 2) (1998) 433–440.
[66] K. Simons, E. Ikonen, Functional rafts in cell membranes, Nature 387 (6633) (1997) 569–572.
[67] B.F. Lillemeier, et al., Plasma membrane-associated proteins are clustered into islands attached to the cytoskeleton, Proc. Natl. Acad. Sci. U. S. A. 103 (50) (2006) 18992–18997.
[68] A. Kusumi, et al., Hierarchical mesoscale domain organization of the plasma membrane, Trends Biochem. Sci. 36 (11) (2011) 604–615.
[69] J.L. Bruses, N. Chauvet, U. Rutishauser, Membrane lipid rafts are necessary for the maintenance of the (alpha)7 nicotinic acetylcholine receptor in somatic spines of ciliary neurons, J. Neurosci. 21 (2) (2001) 504–512.
[70] K. Kizhatil, L.M. Albritton, System y+ localizes to different membrane subdomains in the basolateral plasma membrane of epithelial cells, Am. J. Physiol. Cell Physiol. 283 (6) (2002) C1784–C1794.
[71] P. Robinson, et al., Formation of N-type (Cav2.2) voltage-gated calcium channel membrane microdomains: lipid raft association and clustering, Cell Calcium 48 (4) (2010) 183–194.
[72] A.M. Brainard, et al., Maxi-K channels localize to caveolae in human myometrium: a role for an actin-channel-caveolin complex in the regulation of myometrial smooth muscle K^+ current, Am. J. Physiol. Cell Physiol. 289 (1) (2005) C49–C57.
[73] S. Loebrich, et al., Activated radixin is essential for GABAA receptor alpha5 subunit anchoring at the actin cytoskeleton, EMBO J. 25 (5) (2006) 987–999.
[74] C.M. Hurt, F.Y. Feng, B. Kobilka, Cell-type specific targeting of the alpha 2c-adrenoceptor. Evidence for the organization of receptor microdomains during neuronal differentiation of PC12 cells, J. Biol. Chem. 275 (45) (2000) 35424–35431.
[75] J.T. Goncalves, W. Stuhmer, Calmodulin interaction with hEag1 visualized by FRET microscopy, PLoS One 5 (5) (2010) e10873.
[76] F. Du, et al., Mechanisms for association of Ca^{2+}/calmodulin-dependent protein kinase II with lipid rafts, Biochem. Biophys. Res. Commun. 347 (3) (2006) 814–820.
[77] T. Suzuki, et al., Biochemical evidence for localization of AMPA-type glutamate receptor subunits in the dendritic raft, Brain Res. Mol. Brain Res. 89 (1–2) (2001) 20–28.
[78] V. Von Tscharner, G.K. Radda, The effect of fatty acids on the surface potential of phospholipid vesicles measured by condensed phase radioluminescence, Biochim. Biophys. Acta 643 (2) (1981) 435–448.
[79] X. Han, et al., IgE receptor-mediated alteration of membrane–cytoskeleton interactions revealed by mass spectrometric analysis of detergent-resistant membranes, Biochemistry 48 (27) (2009) 6540–6550.
[80] P.J. Darby, C.Y. Kwan, E.E. Daniel, Caveolae from canine airway smooth muscle contain the necessary components for a role in Ca(2+) handling, Am. J. Physiol. Lung Cell. Mol. Physiol. 279 (6) (2000) L1226–L1235.
[81] E. Balse, et al., Cholesterol modulates the recruitment of Kv1.5 channels from Rab11-associated recycling endosome in native atrial myocytes, Proc. Natl. Acad. Sci. U. S. A. 106 (34) (2009) 14681–14686.
[82] N. Tajima, et al., Activity of BK(Ca) channel is modulated by membrane cholesterol content and association with Na^+/K^+-ATPase in human melanoma IGR39 cells, J. Biol. Chem. 286 (7) (2011) 5624–5638.
[83] K.M. O'Connell, R. Loftus, M.M. Tamkun, Localization-dependent activity of the Kv2.1 delayed-rectifier K^+ channel, Proc. Natl. Acad. Sci. U. S. A. 107 (27) (2010) 12351–12356.
[84] G.A. Fernandez Nievas, F.J. Barrantes, S.S. Antollini, Modulation of nicotinic acetylcholine receptor conformational state by free fatty acids and steroids, J. Biol. Chem. 283 (31) (2008) 21478–21486.
[85] V. Bermudez, et al., Partition profile of the nicotinic acetylcholine receptor in lipid domains upon reconstitution, J. Lipid Res. 51 (9) (2010) 2629–2641.